

Analytical Fresnel laws for curved dielectric interfaces

Sebastian Luhn and Martina Hentschel*

Institute for Physics, Technische Universität Ilmenau, Weimarer Str. 25, 98693 Ilmenau

(Dated: July 11, 2019)

Fresnel laws and the corresponding Fresnel reflection and transmission coefficients provide the quantitative information of the amount of reflected and transmitted (refracted) light in dependence on its angle of incidence. They are at the core of ray optics at planar interfaces. However, the well-known Fresnel formulae do not hold at curved interfaces and deviations are appreciable when the radius of curvature becomes of the order of several wavelengths of the incident light. This is of particular importance for optical microcavities that play a significant role in many modern research fields. Their convexly curved interfaces modify Fresnel's law in a characteristic manner. Most notably, the onset of total internal reflection is shifted to angles larger than critical incidence¹. Here, we derive analytical Fresnel formulae for the opposite type of interface curvature, namely concavely curved refractive index boundaries, that have not been available so far. The accessibility of curvature-dependent Fresnel coefficients facilitates the analytical, ray-optics based description of light in complex mesoscopic optical structures that will be important in future nano- and microphonic applications.

I. INTRODUCTION

The Fresnel equations, derived by Augustine-Jean Fresnel in 1823, quantify the amount of the reflected, R , and transmitted, $T = 1 - R$, intensity of a plane wave incident under a certain angle of incidence χ at a planar interface between two isotropic optical media of refractive indices n_1 and n_2 ². In their original form, they apply to flat interfaces with a relative index of refraction $n = n_1/n_2$. For internal reflection configurations ($n > 1$, reflection at the optically thinner medium) total internal reflection occurs above the critical angle of incidence given by $\chi_{\text{cr}} = \arcsin(1/n)$.

Whereas the effect of the curvature is negligible in many cases when a ray optics description is adequate, it has to be taken into account when the radii a of curvature of the interfaces become as small as several dozens or even several wavelengths λ of the incident light to ensure a reliable description of the reflection and transmission process. This applies for example to optical microcavities with typical sizes of a few dozens micrometers across operated at infrared light^{3,4}. For example, the interface curvature affects, partly via the change in the Fresnel coefficients, the direction of the far field emission of the microcavities^{5,6} as well as semiclassical corrections to the ray picture^{1,7-12}. This implies in particular to deviations from Snell's law as a result of the so-called Fresnel-filtering effect¹³. These deviations have been studied in detail for convexly shaped interfaces based on the analytical Fresnel formulae available in this case^{1,14}.

Here, we derive the missing analytical formulae for concavely curved boundaries as illustrated in Fig. 1. They will provide the basis for a reliable ray-based description of photonic devices with convex or concave interfaces or complex boundaries that combine curved segments of both types. We point out that the analytical Fresnel laws that we present here apply to this general situation. To this end, the local radius of curvature a of the device has to be used in the equations, i.e. the interface at the

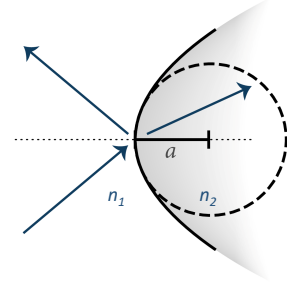


Figure 1. Refraction of light at a concave optical interface between refractive indices n_1 and n_2 corresponding to a relative refractive index $n = n_1/n_2$. The curved interface can be *locally* approximated by a cylinder with radius of curvature a .

point of incidence of the incident ray is approximated by a cylinder (circle) of radius a , cf. Fig. 1.

The paper is organized as follows: We first state the analytical results for the Fresnel equations at curved interfaces (generalized Fresnel laws) both at convex and concave interfaces and discuss the deviations from the planar case. We then outline their derivation based on the transfer matrix approach that nicely illustrates the dual character of the convex-concave reflection situation.

II. FRESNEL REFLECTION COEFFICIENTS AT CURVED INTERFACES

The Fresnel reflection coefficient for the reflected amplitude ratio r of light propagating in a medium with relative refractive index $n > 1$ (internal reflection configuration) with an angle of incidence χ are known to read² for transverse magnetic (TM) and transverse electric (TE, note that we use the convention where TE features the Brewster angle at $\chi_{\text{Br}} = \arctan(1/n)$) polarization, re-

spectively,

$$r_p^{\text{TM}} = \frac{n \cos \chi - \cos \eta}{n \cos \chi + \cos \eta} \quad (1)$$

$$r_p^{\text{TE}} = -\frac{n \cos \eta - \cos \chi}{n \cos \eta + \cos \chi} \quad (2)$$

Here, η is the angle of the transmitted (refracted) light and given by Snell's law via $n \sin \chi = \sin \eta$.

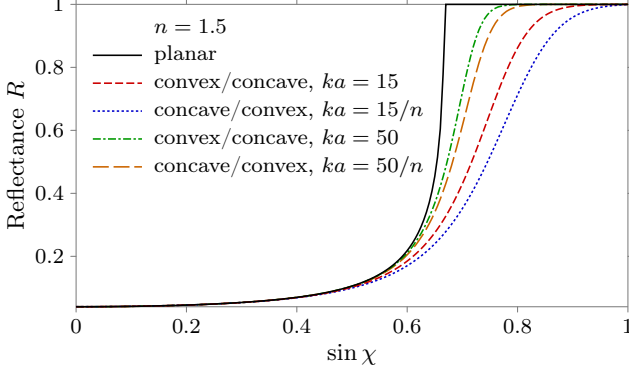


Figure 2. Fresnel reflection coefficients $R = |r|^2, |r_{\text{cx}}|^2, |r_{\text{cv}}|^2$ for TM-polarized light and $n = 1.5$ at planar interface (black) and at curved interfaces with $ka = 50$ (green), and $ka = 15$ (red). Ray path reversal amounts to switching convex/concave and requires to renormalize the wavenumber ka by n (orange and blue curves). Note the delayed onset of total internal reflection as ka is reduced and curvature effects become more dominant.

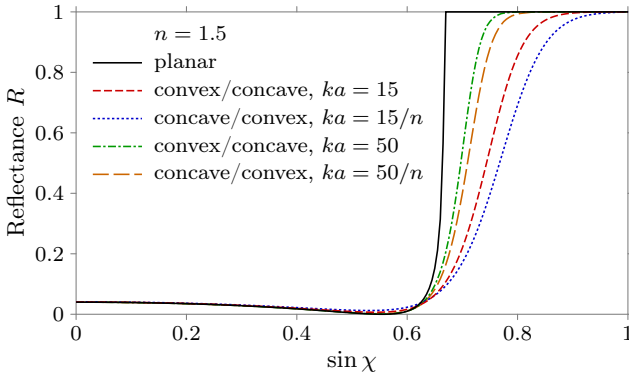


Figure 3. Same as Fig. 2 above, but for TE-polarized light. Note, however, that the Brewster angle reflectivity remains small but finite at curved interfaces. As for the TM-case, deviations from the planar limit are important for reflection above the critical angle $\chi_{\text{cr}} = \arcsin 1/n$ where curved interfaces are more leaky than planar boundaries.

A. Convex case

We shall now see that the backbone structure of these equations is transferred to the curved interfaces. For the convex case, see¹ and the alternative derivation below in

Sec. III, we find the convex Fresnel reflection amplitude r_{cx} (assuming $n > 1$)

$$r_{\text{cx}} = \frac{\cos \chi + i\mathcal{F}_m(ka)}{\cos \chi - i\mathcal{F}_m(ka)}. \quad (3)$$

Here, ka is the dimensionless wave number given as product of the wave number k in free space and the local radius of curvature a . The index m is related to the angle of incidence via $m = nka \sin \chi = ka \sin \eta$ ¹⁵. Furthermore, \mathcal{F}_m is given for TM and TE polarization, respectively, as

$$\mathcal{F}_m^{\text{TM}}(z) = \frac{H_{m-1}^1(z)}{n H_m^1(z)} - \sin \chi \quad (4)$$

$$\mathcal{F}_m^{\text{TE}}(z) = n^2 \mathcal{F}_m^{\text{TM}}(z). \quad (5)$$

B. Concave case

The result for the concave reflection amplitude r_{cv} is the central result of this paper, and has a very similar, noteworthy structure,

$$r_{\text{cv}} = \frac{\cos \chi - i\mathcal{F}_m^*(ka)}{\cos \chi + i\mathcal{F}_m^*(ka)} \quad (6)$$

with the complex conjugation $()^*$ and \mathcal{F}_m as given in Eqs. (4,5). It implies that the reflected intensity $R = |r^2| = rr^*$ is the same at a convex and concave interface, respectively. Note however, that reversal of the light path and the accompanying change from a concave to a convex interface boundary requires to renormalize the wavenumber by n , and the discussion of convex-concave duality below.

The results are illustrated in Figs. 2 and 3 for TM and TE polarized light, respectively. The deviation from the planar case (black curve) is clearly visible and characterized by a much later onset of the regime of total internal reflection (i.e. for angles χ larger than the critical angle χ_{cr}). This effect is more pronounced for smaller wavenumbers ka (higher curvature). The planar case result is approached in the limit $ka \rightarrow \infty$.

The reduced total internal reflection at curved boundaries implies a deterioration of the cavity quality (Q) factor and is thus important for many applications. We also point out that the drop of the reflectivity in TE polarization at the Brewster angle is less pronounced at all curved refractive index boundaries and does, in contrast to the planar case, not (quite) reach zero^{6,12}.

C. External reflection configuration, $n < 1$

Having considered the important case of optical microcavities where $n > 1$, we now generalize the Fresnel equations for curved boundaries to relative refractive in-

dices $n < 1$ and find

$$\tilde{r}_{\text{cx}} = -\frac{\cos \eta + i\mathcal{G}_m^*(ka)}{\cos \eta + i\mathcal{G}_m(ka)} \quad (7)$$

$$\tilde{r}_{\text{cv}} = -\frac{\cos \eta - i\mathcal{G}_m(ka)}{\cos \eta - i\mathcal{G}_m^*(ka)} \quad (8)$$

with

$$\mathcal{G}_m^{\text{TM}}(z) = \frac{n H_{m-1}^2(z)}{H_m^2(z)} \sin \eta, \mathcal{G}_m^{\text{TE}}(z) = \mathcal{G}_m^{\text{TM}}(z)/n^2. \quad (9)$$

The results are shown in Figs. 4 and 5. As before, the reflectivity remains finite around the Brewster angle. The most striking difference to the planar case is the rather low reflectivity near grazing incidence at curved interfaces, confirming their larger leakage that we already observed for $n > 1$.

D. Convex-concave duality

The principle of ray-path reversal as well as the transfer matrix approach outlined below suggest to consider a convex interface together with its concave counterpart as two possible deviations from the planar case for a given n . This implies, however, a renormalization of the reference wavenumber ka in the reversed situation by a factor $1/n$. These results are included in Figs. 2 – 5. In Figs. 2 and 3 the renormalization increases the effect of curvature (the factor n can be captured in a decrease from a to a/n , or alternatively, in an increase from λ to $n\lambda$) and the curves are further away from the ray limit $ka \rightarrow \infty$. For $n < 1$, the same reasoning yields the opposite behavior, cf. Figs. 4 and 5.

To this end we point out a symmetry relation between the convex and concave reflectance for a given order of the Hankel function m : $|r_{\text{cx}}(n \rightarrow n_2)|^2 = |r_{\text{cv}}(n \rightarrow n_2)|^2$, i.e., both coincide and deviate in the same manner from the planar case result. Note however that r_{cx} and r_{cv} differ in a phase such that $r_{\text{cx}}(n \rightarrow n_2) = r_{\text{cv}}^*(n \rightarrow n_2)$. Deviations from this symmetry may occur when light beams that consist of numerous single rays are considered¹¹.

III. TRANSFER MATRICES, RESONANCES, AND FRESNEL COEFFICIENTS

A. The transfer matrix

The transfer matrix relates incoming and outgoing wave amplitudes at (dielectric) interfaces¹⁶, cf. Fig. 6. Here A_0 , B_0 and A_1 , B_1 are the amplitudes of the incoming and outgoing waves, respectively, being related by the transfer matrix M as

$$\begin{pmatrix} A_1 \\ B_1 \end{pmatrix} = M \begin{pmatrix} A_0 \\ B_0 \end{pmatrix} \text{ where } M = \begin{pmatrix} a & b \\ b^* & a^* \end{pmatrix} \quad (10)$$

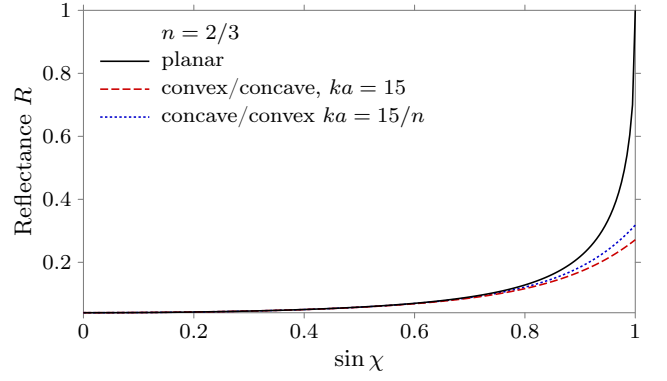


Figure 4. Same as Fig. 2 above, but now for the external reflection configuration, $n < 1$. Note that the reflectivity at curved boundaries remains moderate even at grazing incidence. As before, the planar limit is reached as ka is increased.

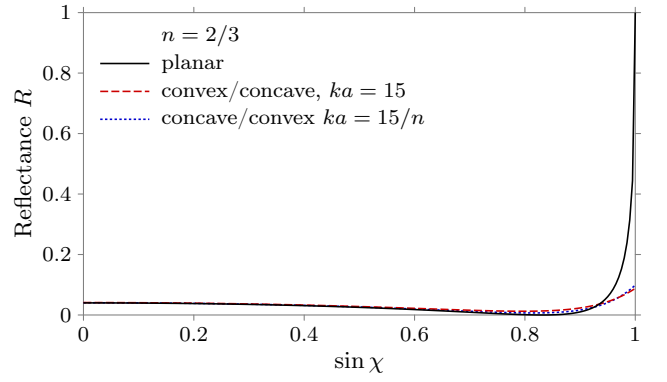


Figure 5. Same as Fig. 4, but for TE-polarized light.

Due to the presence of time-reversal symmetry, the 2×2 matrix M takes the preceding form, where a and b are complex numbers. The relation to Fresnel coefficients is achieved when writing each outgoing amplitude in terms of a reflected and a transmitted contribution, see Fig. 6, that are related by

$$A_1 = r' B_1 + t A_0 \quad (11)$$

$$B_0 = t' B_1 + r A_0 \quad (12)$$

Here r and t (r' and t') are the inner (outer) Fresnel reflection and transmission coefficients, respectively. This yields the following representation of M that holds independent of the curvature of the interface,

$$M = \begin{pmatrix} 1/t'^* & r'/t' \\ r'^*/t'^* & 1/t' \end{pmatrix} \quad (13)$$

B. From the cavity transfer matrix to Fresnel coefficients

In the following we will use the electromagnetic wave functions ψ_0, ψ_1 on either side of the interface (cf. Fig. 6)

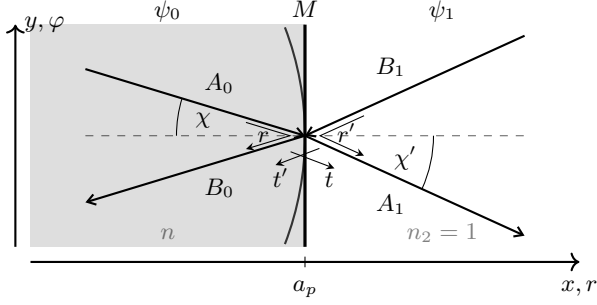


Figure 6. Incident, transmitted, and reflected ray amplitudes are related via the transfer matrix at a curved interface (radius a_p) or a plane. Here, n is the refractive index of the cavity that we assume to be embedded in air. See text for details.

which are nothing else but the z -component of the electric (magnetic) field E_z (H_z) in the TM (TE) case.

Whereas in the planar case the ψ 's are plane waves and a plane divides space into two half planes², a circle/cylinder takes this role in the presence of curvature. Consequently, we use Hankel functions as incoming and outgoing waves ψ because they accommodate the cylindrical symmetry that we assume (locally) for a curved interface.

The derivation of Fresnel coefficients at convex interfaces¹ was based on finding the resonances in a disk cavity, and relating their real and imaginary part to the Fresnel reflection coefficient. Here, we use a conceptually different approach that is applicable to concave interfaces as well. To this end we extend the transfer matrix approach to a Fabry-Perot-type situation with multiple reflections and mimic this behavior by including a perfect mirror, placed at $x, r = 0$. In the case of a planar interface, the plane-wave ansatz for ψ_0 and ψ_1 reads

$$\begin{aligned} \psi_0(x) &= \frac{I}{2} (e^{in_x k_x x} + e^{-in_x k_x x}) \\ &= I \cos(n_x k_x x) \end{aligned} \quad (14a)$$

$$\psi_1(x) = e^{-ik_x x} + S e^{ik_x x}. \quad (14b)$$

The factor I describes (twice) the wave amplitude inside the resonator and S is the transmitted (scattered) amplitude leaving the system. The effective refractive index n_x is given as $n_x = \frac{\tan \chi'}{\tan \chi}$ where χ and χ' are defined in Fig. 6.

Following the procedure outlined in Sec. III A above, the new transfer matrix M' at the position $x = a_p$ reads

$$M' = \frac{1}{t'} \begin{pmatrix} e^{i(n_x-1)k_x a_p} & r' e^{-i(n_x+1)k_x a_p} \\ r' e^{i(n_x+1)k_x a_p} & e^{-i(n_x-1)k_x a_p} \end{pmatrix}. \quad (15)$$

The analogy to the single-transmission case is established by introducing resonance-dressed Fresnel coefficients r_r, r'_r and t_r, t'_r , characterized by the presence of

an additional phase, namely

$$r_r = r e^{2in_x k_x a_p} \quad r'_r = r' e^{-2ik_x a_p} \quad (16)$$

$$t_r = t e^{i(n_x-1)k_x a_p} \quad t'_r = t' e^{i(n_x-1)k_x a_p} \quad (17)$$

A straightforward explanation of the resonance formation is gained when expressing the amplitude I in terms of a geometric series of resonance-dressed Fresnel coefficients, nicely illustrating the successive reflections of light rays,

$$\frac{I}{2} = \frac{t'_r}{1 - r_r} = t'_r + t'_r r_r + t'_r r_r^2 + t'_r r_r^3 + \dots \quad (18)$$

Note that the wave numbers k at resonance can be obtained by solving the equation $1 - r_r = 0$ and that $|I/2|^2$ will oscillate with its maxima reached at resonant wave numbers k .

C. Fresnel coefficients at curved interfaces

We adapt the ansatz for the planar cavity (Eqs. (14a,b)) to the rotationally invariant case relevant for curved interfaces:

$$\psi_0(r, \varphi) = \frac{I}{2} (H_m^1(nkr) + H_m^2(nkr)) = I J_m(nkr) e^{im\varphi} \quad (19a)$$

$$\psi_1(r, \varphi) = (H_m^2(kr) + S H_m^1(kr)) e^{im\varphi}. \quad (19b)$$

Note that we switch from this convex case to the concave situation by exchanging incoming and outgoing Hankel functions (i.e., indices 1 and 2) while properly accounting for the scaling factor n , whereas the distinction between TM and TE polarized light originates in the well-known difference in the transition conditions²:

$$\psi(a_p - 0) = \psi(a_p + 0) \quad (20a)$$

$$\psi'(a_p - 0) = \begin{cases} \psi'(a_p + 0) & \text{TM} \\ n^2 \psi'(a_p + 0) & \text{TE} \end{cases} \quad (20b)$$

The transfer matrix takes then the following form

$$M^{(TM)} = \frac{1}{D} \begin{pmatrix} D_{12} & D_{22} \\ -D_{11} & -D_{21} \end{pmatrix} \quad (21)$$

$$M^{(TE)} = M^{(TM)} + \frac{\sin \chi}{D} \left(n - \frac{1}{n} \right) \begin{pmatrix} -Q_{12} & -Q_{22} \\ Q_{11} & Q_{21} \end{pmatrix} \quad (22)$$

with (realizing that a_p takes the role of a , and $\{\alpha, \beta\} \in \{1, 2\}$)

$$D_{\alpha\beta} = H_m^\alpha(nka) H_{m-1}^\beta(ka) - n H_{m-1}^\alpha(nka) H_m^\beta(ka) \quad (23)$$

$$D = 4/(i\pi ka) \quad (24)$$

$$Q_{\alpha\beta} = H_m^\alpha(nka) H_m^\beta(ka) \quad (25)$$

By analyzing the resonance-dressed (or multiple) reflection coefficients obtained from Eqs. (21, 22), we find

the following additional phases in the Fresnel reflection coefficients (cf. Eqs. (16,17) for the planar case):

$$\text{convex: } \frac{H_m^1(nka)}{H_m^2(nka)}, \quad \text{concave: } \frac{H_m^2(ka)}{H_m^1(ka)} \quad (26a)$$

The resulting reflection coefficient at a **convex** interface reads thus

$$r^{(TM)} = -\frac{\frac{H_{m-1}^1(ka)}{H_m^1(ka)} - n \frac{H_{m-1}^1(nka)}{H_m^1(nka)}}{\frac{H_{m-1}^1(ka)}{H_m^1(ka)} - n \frac{H_{m-1}^2(nka)}{H_m^2(nka)}} \quad (27)$$

This coefficient will not oscillate when changing the argument nka . It is therefore suitable to describe open segment boundaries, in consistency with allowing non-integer $m = nka \sin \chi$ (the integer- m constraint applies formally only in the presence of rotational symmetry).

We proceed by simplifying the expressions using the large-argument approximation

$$\frac{H_{m-1}^1(nka)}{H_m^1(nka)} \approx e^{-i(\chi - \frac{\pi}{2})} = \sin \chi + i \cos \chi, \quad (28)$$

where $\chi = \arcsin(m/nka)$ as before. This relation can be derived using a somewhat less-common approximation for the Hankel function¹⁷ that holds when m and the argument nka of the Hankel function are of similar order as in the present case, namely

$$H_m^1(z) = \frac{\sqrt{2/\pi}}{\sqrt{z \cos \chi}} e^{i\varphi_m(z)} \left(1 - \frac{b_1(z)}{z \cos \chi} + O(z^{-2}) \right) \quad (29)$$

where

$$\varphi_m(z) = z \cos \chi - m \left(\frac{\pi}{2} - \chi \right) - \frac{\pi}{4} \quad (30)$$

and

$$b_1(z) = \frac{1}{8} + \frac{5}{24} \tan^2 \chi. \quad (31)$$

Equation (28) follows in the limit of large m and nka , and eventually we find indeed the results stated in Eqs. (3) and (7).

In analogy, we find for the **concave** case

$$r^{(TM)} = -\frac{\frac{H_{m-1}^-(ka)}{H_m^-(ka)} - n \frac{H_{m-1}^-(nka)}{H_m^-(nka)}}{\frac{H_{m-1}^+(ka)}{H_m^+(ka)} - n \frac{H_{m-1}^-(nka)}{H_m^-(nka)}}. \quad (32)$$

We proceed by simplifying the expressions using the previously introduced approximation for the argument ka being in the order of m , and $\eta = \arcsin(m/ka)$,

$$\frac{H_{m-1}^1(ka)}{H_m^1(ka)} \approx e^{-i(\eta - \frac{\pi}{2})} = \sin \eta + i \cos \eta, \quad (33a)$$

$$\frac{H_{m-1}^2(ka)}{H_m^2(ka)} \approx e^{+i(\eta - \frac{\pi}{2})} = \sin \eta - i \cos \eta. \quad (33b)$$

From this, Eqs. (6) and (8) follow. For the derivation of the TE-case results in Chapter II, we proceed as before but use the appropriate transfer matrix Eq. (22).

To **summarize**, we have completed the picture of Fresnel coefficients at generic curved interfaces by deriving a formulae for the concave case in addition to the previously known convex case coefficients, and by illustrating the power of the transfer matrix approach to this problem.

IV. FUNDING INFORMATION

M.H. acknowledges funding in the DFG Emmy Noether program. We thank Juluis Kullig, Jakob Kreissmann, Henning Schomerus, and Stefan Sinzinger for stimulating discussions.

* Corresponding author: martina.hentschel@tu-ilmenau.de

¹ Martina Hentschel and Henning Schomerus. Fresnel laws at curved dielectric interfaces of microresonators. *Phys. Rev. E*, 65:045603, Apr 2002. doi:10.1103/PhysRevE.65.045603. URL <http://link.aps.org/doi/10.1103/PhysRevE.65.045603>.

² Ariel Lipson, Stephen G. Lipson, and Henry Lipson. *Optical Physics*. Cambridge University Press, 4 edition, 2010. doi:10.1017/CBO9780511763120.

³ Richard K. Chang and Anthony J. Campillo, editors. *Optical processes in microcavities*, volume 3 of *Advanced series in applied physics*. World Scientific, Singapore, 1996. ISBN 9810223447.

⁴ Kerry Vahala. *Optical Microcavities*. World Scientific, Singapore, 2004.

⁵ Harald G. L. Schwefel, Nathan B. Rex, Hakan E. Tureci, Richard K. Chang, A. Douglas Stone, Tahar Ben-Messaoud, and Joseph Zyss. Dramatic shape sensitivity of directional emission patterns from similarly deformed cylindrical polymer lasers. *J. Opt. Soc. Am. B*, 21(5):923–934, May 2004. doi:10.1364/JOSAB.21.000923.

⁶ Daniel Kotik and Martina Hentschel. How curvature affects the far-field emission from deformed optical microcavities. *J. Opt.*, 15(1):014010, 2013. URL <http://stacks.iop.org/2040-8986/15/i=1/a=014010>.

⁷ Henning Schomerus and Martina Hentschel. Correcting ray optics at curved dielectric microresonator interfaces: Phase-space unification of Fresnel filtering and the Goos-Hänchen shift. *Phys. Rev. Lett.*, 96:243903, Jun 2006. doi:10.1103/PhysRevLett.96.243903. URL <http://link.aps.org/doi/10.1103/PhysRevLett.96.243903>.

- ⁸ Eduardo G. Altmann, Gianluigi Del Magno, and Martina Hentschel. Non-Hamiltonian dynamics in optical microcavities resulting from wave-inspired corrections to geometric optics. *EPL*, 84(1):10008, 2008. URL <http://stacks.iop.org/0295-5075/84/i=1/a=10008>.
- ⁹ Julia Unterhinninghofen, Jan Wiersig, and Martina Hentschel. Goos-Hänchen shift and localization of optical modes in deformed microcavities. *Phys. Rev. E*, 78:016201, Jul 2008. doi:10.1103/PhysRevE.78.016201. URL <http://link.aps.org/doi/10.1103/PhysRevE.78.016201>.
- ¹⁰ Julia Unterhinninghofen and Jan Wiersig. Interplay of Goos-Hänchen shift and boundary curvature in deformed microdisks. *Phys. Rev. E*, 82:026202, Aug 2010. doi:10.1103/PhysRevE.82.026202. URL <http://link.aps.org/doi/10.1103/PhysRevE.82.026202>.
- ¹¹ Pia Stockschläder, Jakob Kreismann, and Martina Hentschel. Curvature dependence of semiclassical corrections to ray optics: How Goos-Hänchen shift and Fresnel filtering deviate from the planar case result. *EPL*, 107(6):64001, 2014. URL <http://stacks.iop.org/0295-5075/107/i=6/a=64001>.
- ¹² Pia Stockschläder and Martina Hentschel. Consequences of a wave-correction extended ray dynamics for integrable and chaotic optical microcavities. *Journal of Optics*, 19(12):125603, 2017. URL <http://stacks.iop.org/2040-8986/19/i=12/a=125603>.
- ¹³ Hakan E. Tureci and A. Douglas Stone. Deviation from Snell's law for beams transmitted near the critical angle: application to microcavity lasers. *Opt. Lett.*, 27(1):7-9, Jan 2002. doi:10.1364/OL.27.000007. URL <http://ol.osa.org/abstract.cfm?URI=ol-27-1-7>.
- ¹⁴ Martina Hentschel and Klaus Richter. Quantum chaos in optical systems: The annular billiard. *Phys. Rev. E*, 66:056207, Nov 2002. doi:10.1103/PhysRevE.66.056207. URL <http://link.aps.org/doi/10.1103/PhysRevE.66.056207>.
- ¹⁵ Note1. Note that m is integer only for cylindrical resonators where it is the angular momentum quantum number and is directly related to the order of the Hankel Functions¹⁴. In the general case we are interested here m is related to the expectation value of the angle of incidence. Hankel functions of non integer order are well defined¹⁸ and ensure the continuous behavior of the Fresnel coefficients, e.g. $J_\nu(x) = \sum_{\nu=0}^{\infty} (-1)^\mu \frac{(x/2)^{2\mu+\nu}}{\Gamma(\mu+1)\Gamma(\mu+\nu+1)}$.
- ¹⁶ Max Born and Emil Wolf. *Principles of Optics*. Cambridge University Press, 7 edition, 1999.
- ¹⁷ A. Erdélyi. *Higher Transcendental Functions*, volume II. McGraw-Hill, 1955.
- ¹⁸ Dr. Wilhelm Magnus, Dr. Fritz Oberhettinger, and Dr. Raj Pal Soni. *Formulas and Theorems for the Special Functions of Mathematical Physics*. Springer-Verlag Berlin Heidelberg, 1966.